Interaction of NO₂ with Hydrocarbon Soot: Focus on HONO Yield, Surface Modification, and Mechanism

Daniel G. Aubin and Jonathan P. D. Abbatt*

Department of Chemistry, University of Toronto, 80 St. George Street, Toronto, Ontario M5S 3H6, Canada

Using a coated-wall flow tube connected to a mass spectrometer, the heterogeneous conversion of NO_2 to HONO on dry hydrocarbon soot surfaces has been studied at room temperature and 243 K. Particular attention was given to the measurement of the HONO yield as a function of hydrocarbon fuel, NO_2 partial pressure, extent of uptake, and surface oxidation state. In all cases, the yield is invariant of these parameters and close to unity, indicative of an irreversible oxidation mechanism by which the NO_2 abstracts an H atom from the surface. XPS analysis shows that the surface N content does not measurably increase with NO_2 exposure. There is minimal surface reactivity regeneration with time or via exposure to high relative humidity. A BET surface area measurement of the entire soot film exposed to NO_2 was used to determine the amount of HONO that can be generated from the soot surface per unit surface area, prior to its deactivation. The reduction of NO_2 to HONO on soot is unlikely to account for the observed nighttime buildup of HONO in polluted urban environments.

Introduction

Heterogeneous processes occurring on the surface of aerosols can alter atmospheric composition by acting as a sink or source of gas-phase species.[1] One such material is soot or black carbon (BC) aerosols that have anthropogenic sources such as fossil fuel combustion and natural sources such as biomass burning.[2] Loadings of BC in the boundary layer range from 1.5 to 20 μg m^{-3} (urban) to 0.2−2 μg m^{-3} (rural),[3] but decrease to 5−20 ng m^{-3} over the ocean areas[4−7] and to 1 ng m^{-3} over the Poles.[8] Even though BC generally constitutes a small fraction of the total aerosol mass, which can be up to tens of percent, its fractal and porous surface when freshly emitted leads to a considerably larger contribution to the total aerosol surface area.[9−11] Several studies have examined the chemical functionalities present on soot surfaces,[12−17] given that the reactivity of soot depends on the nature of the surface functional groups present.[18] For example, Akhter et al. have shown for laboratory-generated soot that there are many different polycyclic aromatic hydrocarbons (PAHs) condensed onto a carbon backbone, which has alcohol, anhydride, carbonyl, carboxyl, and ether functional groups at its surface.[12,13]

The reactions of nitrogen oxides on soot have attracted recent attention due to their potential to influence the NO_x/HNO_3 ratio and HO_x budget.[1,19,20] The reactive uptake of NO_2 leading to the formation of HONO has been observed extensively[21] and has been proposed by some to explain the high buildup of HONO during the nighttime in polluted environments.[22−24] Various products have been reported for this reaction, including HONO, the yield of which has been observed to vary as a function of NO_2 concentration, relative humidity, and soot combustion conditions.

Average nighttime HONO concentrations in urban areas are 1−15 ppb, which drop to 1 and 0.1 ppb in rural and remote areas, respectively.[25] For polluted environments, the photolysis

of HONO in the early morning can be a major HO_x source when other formation mechanisms, such as HCHO and O_3 photolysis, are less efficient. One field study in Milan determined that during the first 4−6 h after sunrise, HONO photolysis is the most important OH source in the boundary layer and that HONO can account for up to 34% of the total OH formation.[26] Recently, there have been a number of field studies that have provided evidence for a strong daytime source of HONO.[27−29]

Despite HONO's importance, its formation mechanism remains poorly quantified. Gas-phase radical chemistry cannot explain the observed HONO levels at night. Measurements of direct emission of HONO from combustion sources show that the HONO/NO_x ratio is too small (from 10^{-4} to 10^{-2}) to explain the ratio measured in the boundary layer.[30,31] On the other hand, heterogeneous processes have long been known to form HONO.

Early laboratory experiments have observed the formation of HONO from the reaction of NO_x with H_2O on glass, Pyrex, and Teflon, suggesting a heterogeneous reaction.[32] A possible mechanism is

$$2NO_2 + H_2O \rightarrow HONO + HNO_3 \qquad (1)$$

However, this mechanism is inconsistent with laboratory studies involving soot, in which HNO_3 was not detected as a product, the reactivity of soot was depleted upon exposure, and HONO yields >50% were observed.[23,33−36] This has led to reaction 2 being proposed as a reduction−oxidation process by which the soot surface reduces NO_2 to HONO.[22,23]

$$NO_2 + RH \rightarrow HONO + R \qquad (2)$$

Some of the carbonaceous surfaces investigated include commercial black carbon such as Degussa FW2 and Printex,[36−42] spark discharge soot generated from graphite electrodes,[22,39,43−45] gaseous hydrocarbon soot, such as methane, propane, and acetylene,[23,24,33] liquid hydrocarbon soot such as hexane, decane, toluene, and diesel,[23,24,33−35,41,42,44,46,47] power plant aerosols,[48]

* Author to whom correspondence should be addressed (e-mail jabbatt@chem.utoronto.ca).

amorphous carbon,[38,48] and organic carbon.[49] Almost all experiments using BC and soot as a substrate have shown a reactive uptake of NO_2[22−24,33−41,43,44,46,48,50] with the formation of NO[23,33−41,43,48] and HONO.[22−24,33−36,41,43,46−48,50] The reaction is noncatalytic, although some regeneration of reactivity was observed upon heating[23] or exposure of the sample to H_2O.[24]

Despite considerable research on this topic, there remain outstanding uncertainties in the kinetics and atmospheric importance of this process. In particular, a very wide range of uptake coefficients has been reported, from 0.1 to 10^{-8}. Many of the experiments were conducted on substrates for which the specific surface area was not addressed or was estimated, which would lead to an uncertainty in the uptake coefficient and HONO generation capability because the specific surface area of soot can be orders of magnitude larger than the sample's geometric area. Considerable ambiguity in the mechanism arises from the range of observed HONO yields, from 0 to 100%. This range may arise from the variety of experimental conditions used. For example, experiments conducted at very high NO_2 concentrations may promote reaction 1 over reaction 2, and the use of calibrations in which HONO is not directly measured can lead to inaccuracies in the measured HONO concentrations.

In this work we attempted to address these uncertainties in the uptake kinetics and HONO yields, and so gain a better understanding of the overall mechanism for NO_2 uptake on soot. In particular, we examined the reactive uptake of NO_2 using atmospherically relevant NO_2 concentrations on a large number of *n*-hexane, decane, and benzene soot samples for which the specific surface area was measured. HONO yields relative to both loss of NO_2 and the total soot surface area were measured. The oxidation state and elemental composition of the soot surfaces were determined using XPS both before and after exposure to NO_2 and O_3 in order to determine changes in the surface chemistry. We also studied how O_3 oxidation affects the reaction kinetics.

Experimental Section

Soot was formed from an *n*-hexane, benzene, or decane diffusion flame, where a burner is housed in a water-cooled chimney provided with an air flow of 10−15 SLPM. The soot was deposited on the inner walls of a 20 cm long, 2.3 cm i.d. Pyrex tube held 5−10 cm above the tip of the burner. The soot was deep black in color, and the mass deposited ranged from 0.088 to 0.819 g. The specific surface area (SSA) of the entire film was determined by measuring the BET adsorption isotherm of Kr at 77 K.[51] In particular, the soot-coated Pyrex tube was placed in a 22 cm long, 3 cm i.d. stainless steel cylinder equipped with copper gasket seals that was then immersed in liquid nitrogen. The soot was exposed to different known amounts of Kr. The number of moles of Kr adsorbed to the soot surface was obtained from the difference in the final pressure after the soot sample had been exposed to Kr and that which would have been obtained from the expansion of the Kr into an empty chamber. Control experiments showed the Pyrex surface presents negligible surface area. The surface area was determined from the linear form of the BET isotherm using the method recommended by IUPAC.[52]

The uptake experiments were conducted in a low-pressure, coated-wall flow tube coupled to an electron-impact mass spectrometer, shown in Figure 1, similar to that used previously to measure the adsorption of HNO_3 and PAHs onto *n*-hexane soot films.[53,54] The soot-coated tube was inserted into a double-jacketed flow tube through which a flow of 400−450 sccm of helium carrier gas (high-purity grade, Air Products) at 0.77 Torr
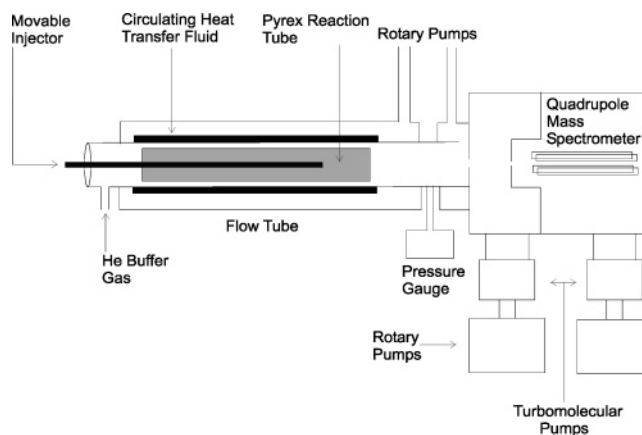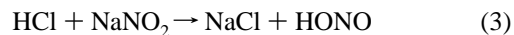

Figure 1. Diagram of the coated-wall flow tube coupled to an electron-impact mass spectrometer used in the uptake experiments.

was established for 10−15 min prior to the beginning of an experiment. The uptake experiments were conducted at 243 K and ambient temperature by using a low-temperature circulating bath.

A differentially pumped electron-impact mass spectrometer (UTI) sampled the composition of the gas exiting the flow tube by monitoring m/z 46 for NO_2 and m/z 47 for HONO. HONO does not fragment to give a signal at m/z 46, and isotopically heavy NO_2 or HONO impurities in the NO_2 contribute only a small signal to m/z 47. We initially monitored m/z 63 as well to detect HNO_3, but we did not notice an increase in the signal at m/z 63 when NO_2 was added to the flow tube, constraining the HNO_3 content of our NO_2 bulb to be no more than 5% on the basis of literature values for the ratio of intensity at m/z 46 to that at m/z 63 and our estimated detection limits.[53,55] The electron energy was 70 eV, and the data were recorded at 2.6 s intervals.

NO_2 was added to the flow tube through a movable injector initially positioned with its tip beyond the downstream end of the soot film. In all cases, the flow exiting the injector tip never exceeded 10% of the total flow, which ensured that mixing into the bulk flow was rapid. The partial pressure of NO_2 was determined from the pressure drop with time from a glass reservoir containing dilute NO_2 (Matheson Gas) in helium. The uptake experiments were conducted by pulling the injector back over the soot film by a distance of 10, 15, or 20 cm, the exact value being determined by the need to see a sufficiently large change in signal. The injector was then pushed back to the starting position as the NO_2 signal leveled off. The loss of signal after withdrawal of the injector was integrated to determine the amount of NO_2 lost to the surface. By referencing this amount to the surface area exposed, a total uptake is determined. By measuring the decline in signal immediately after withdrawal of the injector, an initial uptake coefficient (γ_0) can also be obtained.[56] Control experiments were conducted on a bare Pyrex tube, and no uptake of NO_2 or formation of HONO was observed.

The mass spectrometer detection limits were 2×10^{-6} and 7×10^{-6} Torr for NO_2 and HONO for 0.52 s integration times per mass, respectively. The mass spectrometer was calibrated for HONO at m/z 47 using a HONO source modified from that of Febo et al., which is shown in Figure 2.[57] HONO was prepared by flowing a known quantity of gaseous HCl diluted in helium from a bulb into a damp bed of $NaNO_2$ deposited on a frit in a vertical flow cell. This leads to HONO formation via

$$HCl + NaNO_2 \rightarrow NaCl + HONO \tag{3}$$

Interaction of NO$_2$ with Hydrocarbon Soot

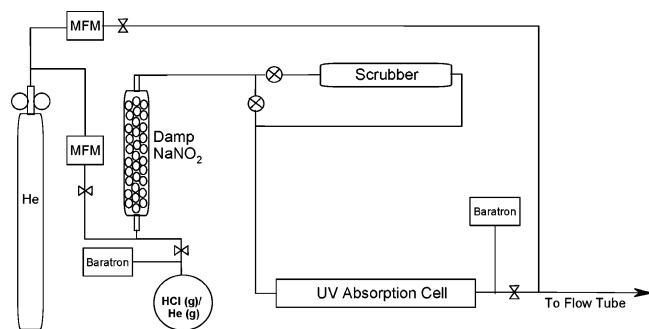*J. Phys. Chem. A, Vol. 111, No. 28, 2007* **6265**

Figure 2. Diagram of the HONO generation source and detection system (MFM, mass flow meter).

HCl is known to react efficiently with HONO to yield ClNO and H$_2$O in the gas phase.[58] However, we observed no mass spectrometer signal for HCl or ClNO, indicating that there was no HCl breakthrough under our experimental conditions. Febo et al. observed the occurrence of the following two HONO loss processes[57]

$$2HONO \rightarrow NO + NO_2 + H_2O \qquad (4)$$

$$HONO + NO_2 \rightarrow NO + HNO_3 \qquad (5)$$
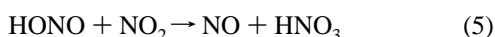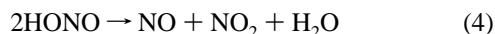
with reaction 4 dominating. At high pressures in the cell we observed the HONO-to-NO$_2$ ratio decreasing below the value at lower pressures, probably because reaction 4 was proceeding. As a result, we ran the source at a low pressure of roughly 50 Torr.

The HONO concentration was determined in the source using absorbance at 254 nm, at which HONO's absorbance cross section is 11 times larger than that of NO$_2$.[59] The absorbance cell was 54 cm long and 3.1 cm i.d. and was equipped with quartz windows at each end. The radiation from a mercury Pen-Ray lamp (UVP Inc.) first passed through an interference filter isolating the 254 nm line, then through a lens, the absorption cell, another lens, and onto a silicon carbide photodetector (Boston Electronics Corp.). A second beam of light from the same Pen-Ray lamp passed through a second interference filter and onto a reference photodiode. To reduce the noise in the mercury lamp's signal due to short time scale fluctuations, the ratios of the signal from the main and the reference photodiode were taken. The signal intensities from the photodiodes were sampled using a commercial data acquisition board.

For calibration, we used HONO partial pressures in the flow tube of 5×10^{-5}–2×10^{-4} Torr to have a sufficiently large absorbance signal of 0.4–1.4%. Specifically, the partial pressures were determined from this absorbance signal and from the pressure drop and dilution that occur when the HONO flow passed into the low-pressure flow tube. The partial pressures in the calibration were just slightly above the HONO concentration range generated by exposing the soot samples to 10^{-5}–10^{-4} Torr of NO$_2$. Under the same flow tube conditions and on the same day, the NO$_2$ sensitivity was determined by measuring the drop in pressure in time from the NO$_2$ reservoir. The ratio of the mass spectrometer sensitivity to NO$_2$ at *m/z* 46 and HONO at *m/z* 47, which was 3.5 ± 0.5 (where all precision errors in the paper are 1 − σ standard deviation uncertainties), was used to determine the HONO concentrations in the flow tube, and this ratio remained constant through months of experiments. For the yield experiments, we extrapolated the S_{46}/S_{47} ratio to lower partial pressures given the linearity of the calibration under the higher partial pressure conditions. Overall, we estimate the

errors in the HONO yields to be ±20%, arising primarily from the errors in this ratio and in the absorption coefficient for HONO.[59]

For the soot oxidation experiments, ozone was prepared by photolyzing oxygen (Air Products, Extra Dry Grade) diluted in nitrogen (Grade 4.8 BOC Edwards) flowing through a cell irradiated with a UV lamp at 185 nm (Jelight Co. Inc., model 100). The concentration of the ozone in the bulb was determined by measuring the absorbance at 254 nm. The resulting mixture of ozone, oxygen, and nitrogen then flowed through a flow tube containing the soot film. Chemical analysis of the hexane soot using a Thermal Optical Transmission instrument (Sunset Laboratory Inc.) showed that it was largely elemental carbon, with an elemental carbon (to total carbon) fraction ranging from 0.86 to 0.94. For a more detailed account of the procedure refer to Fan, Brook, and Mabury.[60]

Selected soot samples were analyzed by X-ray photoelectron spectroscopy (XPS) at the Surface Interface Ontario facility to obtain the surface elemental composition of carbon, oxygen, and nitrogen. XPS spectra were taken for fresh benzene, hexane, and decane soot and for benzene soot exposed to low and high concentrations of NO$_2$, to a mixture of NO$_2$ with O$_2$, and to O$_3$. The XPS spectra were obtained on a Leybold MAX 200 XPS system (LH, Cologne, Germany) using an unmonochromatized Al Kα source operating at 1486.6 eV. The energy range was calibrated against Cu 2p$_{2/3}$ and Cu 3p lines at 932.7 and 75.1 eV, respectively. The energy scale was corrected by placing the C 1s value for the main C−C component at 285 eV. Atomic ratios were obtained from spectra collected in a low-resolution mode (PE = 192 eV). Empirically derived sensitivity factors, also supplied by the manufacturer, appropriate for these spectra (C 1s = 0.31, O 1s = 0.75, N 1s = 0.54) were used.

Once it was determined that the magnitude of the uptake coefficient and the yields were very similar for all three hydrocarbon soot substrates, benzene soot was used for the experiments dealing with humidification, regeneration of reactivity, ozonation, and high NO$_2$ dose because a benzene flame produces the most soot, making it easier to generate a large number of soot samples.

Results and Discussion

Specific Surface Area. To be able to report the total HONO yield per unit soot surface area on the molecular scale, we measured the SSA for selected samples of hexane, decane, and benzene soot deposited on the inside of the Pyrex tube. As opposed to measuring a small sample of the film hoped to be representative of the bulk, this is a more appropriate approach because we obtain the total amount of surface area available to interact with NO$_2$. The measured ratio of the SSA to the geometric area ranged from 255 to 709.

Figure 3 shows a plot of the SSA as a function of sample mass for several hexane, decane, and benzene soot films. For the sample masses used we were in the linear mass versus surface area regime, with no observed saturation of the surface area. This means that the entire soot surface in the samples was available and there were no underlying inaccessible soot layers. Furthermore, all three substrates have nearly the same slope, the average being 15 ± 1 m^2 g^{-1}. This is surprising considering that all three soot films appeared to the eye to be different when deposited on the inside of the Pyrex tube. For example, benzene soot formed a thicker and rougher coat, whereas the hexane film was thin and even.

NO$_2$ Uptake Profile. In Figure 4, we present an uptake profile for NO$_2$ on a 0.351 g benzene soot film at room
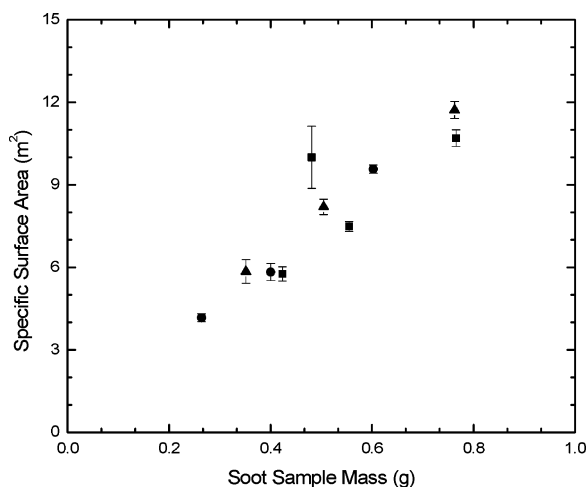
Figure 3. Specific surface area for selected soot samples as a function of sample mass as determined from the BET isotherm (square, hexane; triangle, benzene; circle, decane). The slope from the linear fit was found to be $15 \pm 1 \ m^2 \ g^{-1}$.

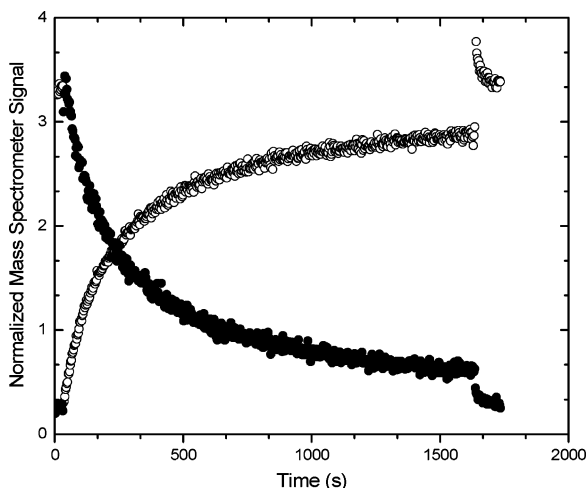**Figure 4.** Sample uptake profile of NO_2 (open circle) on a 0.351 g benzene soot film at room temperature with an NO_2 partial pressure of 4.6×10^{-5} Torr. The HONO (solid circle) signal has been normalized to NO_2 by multiplying by 3.5.

temperature. This profile is typical of soot from all three fuels, and such profiles form the basis of all experimental results to be presented. The NO_2 partial pressure ranged from 8×10^{-6} to 1.4×10^{-4} Torr, which is equivalent to $10-130$ ppb at atmospheric pressure. These are appropriate partial pressures for urban locations,[2,61] whereas a number of previous studies have been done using higher NO_2 partial pressures that are unrepresentative of the atmosphere.[41,42,44] Choi and Leu have shown that for the uptake of HNO_3 at high partial pressures, which results in high surface coverages, bimolecular surface reactions can occur, which otherwise would not at lower HNO_3 concentrations typical of an urban environment.[62] Presumably similar effects may arise with NO_2 under unrealistically high concentration conditions. In addition, high partial pressures of NO_2 may lead to rapid saturation of surface sites on the experimental timescale.

The initial drop in the NO_2 signal in Figure 4 at 31 s corresponds to when the injector was pulled back, thus exposing the soot sample to the NO_2, which then partitions to the surface. We observe a simultaneous rise in the HONO signal at m/z 47. At first, there is rapid uptake of NO_2, followed by a slow asymptotic recovery in the NO_2 signal and a decrease in the

formation of HONO as the surface begins to deactivate. We interpret this slow recovery in the NO_2 signal to be due to the consumption of the reactive sites on the film, plus there may be a component due to NO_2 diffusing into the soot structure and accessing reactive sites deeper within the film. The decrease in pressure over time in the bulb containing the NO_2 generally prevented us from measuring the uptake profile beyond 30 min because the flow of NO_2 leaving the bulb would decrease over time, which would result in a steadily decreasing partial pressure of NO_2 in the flow tube. When the injector is brought back to its initial position, there is a small peak in the m/z 46 signal, which may be due to a small amount of physisorbed NO_2 desorbing from the surface or from HNO_3 desorption if there is a small impurity present. There is also a nearly instantaneous drop in the HONO signal. The time scale for NO_2 desorption and cessation in HONO production is less than the 1 or 2 s needed to push the injector forward. The amount of physisorbed NO_2 or HNO_3 was on average 2% of the total NO_2 taken up, and no more than 5%.

A few low-temperature uptake experiments were conducted at 243 K, and although there was comparable uptake of NO_2 as observed at room temperature, the formation of HONO was suppressed under dry conditions. The uptake of NO_2 was not due to simple physical adsorption as there was no large NO_2 desorption peak when the injector was pushed in. We performed the following experiment as additional confirmation. Half of a film was exposed to NO_2 at room temperature. The film was then rotated in the flow tube, and the other half was exposed to NO_2 at 243 K. Both the low-temperature and room temperature uptakes were similar. However, when the film that had been exposed to NO_2 at low temperatures was warmed to room temperature, pumped upon, and then re-exposed to NO_2, only 45% of the uptake at low temperature was observed. Had physical adsorption of NO_2 been occurring, we would have expected the uptake to be unaffected because the NO_2 would have desorbed at room temperature. Instead, we believe that the low HONO yield at low temperature arises from it remaining adsorbed on the surface after formation. Either it does not desorb upon our experimental time scales, or else it builds up on the surface so that a reaction such as (4) proceeds.

HONO Yield. The main focus of this paper is to quantify the HONO yield, relative to NO_2 loss, to better define the reaction mechanism and also to evaluate the maximum contribution that such soot chemistry may have on nighttime HONO concentrations in the atmosphere. Figure 5 shows the yields of HONO, defined as the number of HONO molecules produced for every NO_2 molecule taken up, on hexane, decane, and benzene soots. The HONO yields, similar for all three substrates, were $96 \pm 18\%$ for a total of 51 films (see Table 1). The uncertainty quoted is the $1 - \sigma$ precision uncertainty. We estimate the instrumental error arising from determining the NO_2 and HONO concentrations in the flow tube to be $\pm 14\%$. In particular, some of the scatter in the plots arises from integration of small signals associated with HONO, given that our sensitivity for its detection is lower than for NO_2. Some of the variability may arise from film to film variations as well. Finally, the small amount of NO_2 physically adsorbed to the soot surface, which was $\leq 5\%$ of the total NO_2 taken up, could lead to a low and perhaps variable bias in our reported yields; that is, some of the NO_2 adsorbs but does not react away. This desorption area was not always measured in our experiments, and so we made no attempt to correct for it.

The HONO yield was found to be invariant with the partial pressure of NO_2 used (Figure 6), the extent of NO_2 uptake to

Interaction of NO₂ with Hydrocarbon Soot

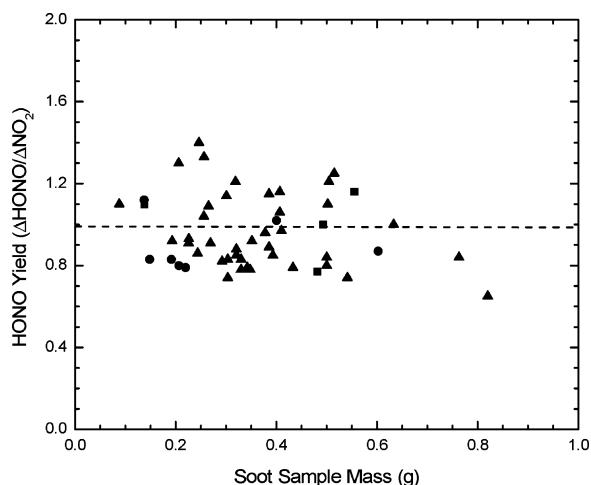*J. Phys. Chem. A, Vol. 111, No. 28, 2007* **6267**

Figure 5. HONO yields determined on all hexane (square), decane (circle), and benzene (triangle) soot films at room temperature. Dashed line represents the average yield for all samples of 96 ± 18% (1 − σ precision).
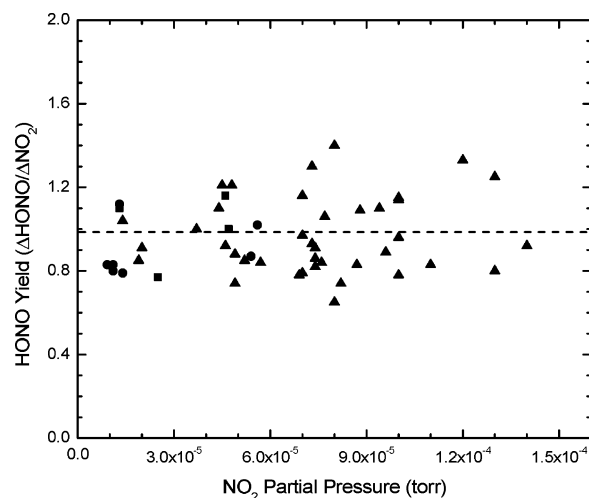

Figure 6. HONO yields determined on all hexane (square), decane (circle), and benzene (triangle) soot films as a function of NO₂ partial pressure. Dashed line represents the average yield for all samples of 96 ± 18 % (1 − σ precision).

the surface (Figure 7), or multiple NO₂ exposures to the same film (Table 2, see Regeneration of Reactivity and Effect of Water), via humidification of the soot film (see Regeneration of Reactivity and Effect of Water) or after oxidation of the soot film with ozone (Table 3) even though the NO₂ uptake decreased greatly.

A comparison of literature HONO yields (Table 1) shows values ranging from 0 to 100%. At the high end of this range, our results are in reasonable agreement with the works of Gerecke et al.,[23] Kleffmann et al.,[41] Alcala-Jornod et al.,[33] Stadler et al.,[34] Salgado and Rossi (soot from fuel-rich flames),[35]

and Karagulian and Rossi,[47] whereas considerably smaller yields are reported by Longfellow et al.,[24] Al-Abladeh and Grassian,[50] and Lelievre et al.[46] The wide variability can arise from a number of sources. One of these is temperature; our work confirms earlier reports that the yield decreases at lower temperatures. We attribute this effect to HONO remaining adsorbed on the soot surface after being formed, and it could be the reason why Longfellow et al. report low yields of between 10 and 30% on methane, propane, kerosene, and hexane soot at 262 K.[24] Specifically, for methane and propane soot the room temperature HONO yields were factors of 1.6 and 1.3 times

TABLE 1: Summary of the Literature Data for the HONO Yield for NO₂ Uptake on Soot

| reference	substrate	HONO yield (%)	temperature (K)	NO₂ pressure (Torr)
Tabor et al.[37]	Degussa FW2	0	ambient	10^{-3}
Tabor et al.[38]	FW2 Printex 60 Lamp Black FS101	0	ambient	$(0.08-8) \times 10^{-3}$
Rogaski et al.[40]	Degussa FW2	0	298	$(0.5-10) \times 10^{-3}$
Gerecke et al.[23]	ethylene acetylene toluene	63 ± 4 72 ± 5 91 ± 6	ambient	$2.4 \times 10^{-6}-4.2 \times 10^{-4}$
Longfellow et al.[24]	methane propane kerosene hexane	13 ± 5 10 ± 5 17 ± 5 30 ± 10	262	$(0.6-6) \times 10^{-5}$
Kleffmann et al.[41]	commercial carbon black	50−80	ambient	$7.6 \times 10^{-4}-3 \times 10^{-2}$
Al-Abladeh and Grassian[50]	hexane	36 ± 5	295	7.8×10^{-6}
Alcala-Jornod et al.[33]	toluene acetylene decane	68−99 2−6 58−95	ambient	pulsed dose of $(1-120) \times 10^{14}$ molecules
Stadler et al.[34]	decane (fuel-rich flame) hexane (oxidant-rich flame)	100 a few percent	298	$2.2 \times 10^{-6}-2.6 \times 10^{-4}$
Salgado and Rossi[35]	hexane ($\lambda = 0.16$) hexane ($\lambda = 0.82$)	30 50−80	ambient	$(0.6-3) \times 10^{-5}$
Lelievre et al.[46]	toluene kerosene hexane	30 ± 5	240−350	$(0.28-3.4) \times 10^{-4}$
Kleffmann et al.[36]	Lamp Black	60	ambient	$(3.8-4.5) \times 10^{-4}$
Karagulian and Rossi[47]	decane (fuel-rich flame)	100 ± 10	298	7×10^{-5}
this study	hexane decane benzene	96 ± 18	ambient	$(0.08-1) \times 10^{-4}$
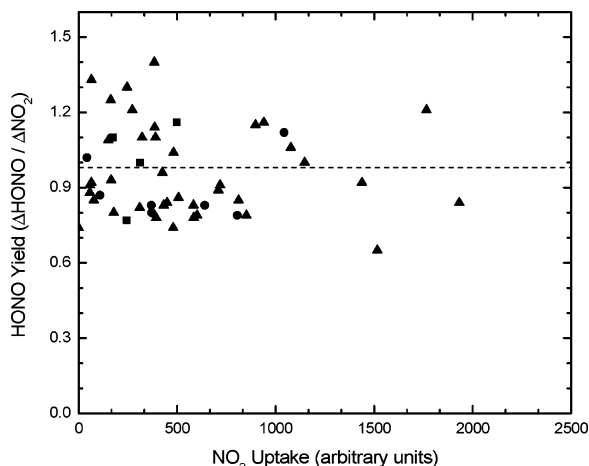
Figure 7. HONO yields determined on all hexane (square), decane (circle), and benzene (triangle) soot films as a function of NO₂ uptake (arbitrary units). Dashed line represents the average yield for all samples of 96 ± 18 % (1 − σ precision).

TABLE 2: NO₂ Uptake on Benzene Soot at Room Temperature as a Function of Multiple Exposures over a Series of Days

film (g)	day	NO₂ uptake (normalized to initial exposure)	HONO yield
0.257	1	1.00	1.03
	3	0.15	1.10
	7	0.14	1.05
	9	0.06	1.18
0.370	1	1.00	0.95
	2	0.21	0.79
	5	0.16	0.92

TABLE 3: NO₂ Uptake on Benzene at Room Temperature Soot after Ozonation

film (g)	O₃ dose (Torr day⁻¹)	NO₂ uptake (normalized to initial exposure)	HONO yield (normalized to initial exposure)
0.410	8.6×10^{-5}	0.75	0.58
0.246	8.6×10^{-5}	0.50	0.66
0.348	3.2×10^{-4}	0.41	1.12
0.206	3.2×10^{-4}	0.47	0.97
0.342	5.8×10^{-4}	0.52	1.05
0.269	5.8×10^{-4}	0.93	0.50
0.502	3.0×10^{-3}	0.45	1.18
0.292	3.9×10^{-3}	0.38	1.23

higher than at 262 K, respectively. However, it does not explain the discrepancy with the work of Lelievre et al.[46] and Al-Abladeh and Grassian,[50] who performed their studies at room temperatures.

Another factor that might affect the HONO yields are the combustion conditions of the flame,[23,34,35] whereas the type of fuel has little effect. Gerecke et al.[23] has shown that the HONO yield decreases for soot collected further away from a flame base, which translates to a more aged and oxidized soot, with the percent HONO yield ranging from 93 ± 1% at the base to 69 ± 5% at the top of the flame. Stadler and Rossi have shown that decane soot produced from a fuel-rich flame yields HONO with up to 100% yields, whereas soot produced from an oxidant-rich flame produced minimal amounts of HONO.[34] Alcala-Jornod, van den Bergh and Rossi, and Stadler and Rossi have shown that the low HONO yields do not imply that HONO is not being produced but that it is being rapidly decomposed on the soot surface, yielding NO.[33,34] This was indicated in HONO uptake experiments in which HONO interacting with toluene

and decane soot led to 5−25% loss of HONO, whereas 90% of the HONO reacted with acetylene soot.[33] Likewise, HONO was found to decompose on decane soot formed from an oxidant-rich flame, whereas HONO was not found to decompose on decane soot produced from a fuel-rich flame.[34] Overall, these observations imply that HONO is being produced in high yields on all types of soot but that it is being decomposed on the surface in the case of more oxidized soot, such as that formed from an oxidant-rich fuel mixture or that produced from a short-chain hydrocarbon such as acetylene. Mechanistically, this is an important conclusion because it suggests that the low HONO yields observed in certain studies may arise from HONO decomposition after its formation rather than from a different HONO production pathway on the surface.

The average amount of HONO generated per unit area was $(8.2 \pm 1.1) \times 10^{13}$ molecules cm⁻² (to the point where the NO₂ signal has recovered to 85% of its starting value), which is close to the saturated surface coverage of 2×10^{14} molecules cm⁻² that we have observed for HNO₃ physical adsorption on n-hexane soot.[53] Our observed value for the density of surface reactive sites is slightly smaller than what has been observed previously by Ammann et al.[22] (3×10^{14} reactive sites cm⁻² on spark discharge soot aerosols), Kirchner et al. (2.2×10^{14} reactive sites cm⁻² on diesel and spark discharge soot),[44] and Kleffmann et al. (10^{14} reactive sites cm⁻² on lamp black),[36] but it is slightly higher than the results of Lelievre et al.[46] [$(3.1 - 4.8) \times 10^{13}$ reactive sites cm⁻² hexane, toluene, and kerosene soot]. This suggests that roughly one-third of the adsorptive sites on these soot surfaces are reactive.

Regeneration of Reactivity and Effects of Water. Table 2 shows the results of two experiments conducted to evaluate if the reactivity of benzene soot could be regenerated. If regeneration is observed, this will increase the overall impact of this reaction on the atmosphere. The uptake of NO₂ was measured on several films up to 8 days after an initial exposure to sufficient doses of NO₂ that the HONO production dissipated, the NO₂ ceased being taken up by the surface, and the mass spectrometer signal for NO₂ reached a plateau. Between the exposures the films were kept undisturbed in the flow tube, which had been filled with room air. After the initial exposure, the subsequent uptake of NO₂ on the following days never exceeded 21% of that from the initial exposure and generally kept decreasing after each subsequent exposure. In all cases the HONO yield was similar to that on the fresh surface, which suggests that there is no change in the reaction mechanism. Longfellow at al.[24] showed that after methane soot is deactivated, it can be reactivated by exposing the system to water with a relative humidity of 4.3%. We performed a similar experiment on benzene soot films by depleting their reactivity and then measuring the uptake on the films 3 days after the initial exposure, and following this we measured the uptake after humidifying the films at 100% relative humidity for 90 min. No regeneration of reactivity was observed under dry conditions after the initial exposure or after humidification, in which case the reactivity decreased even further.

Because our experiments were conducted with a dry helium carrier gas, this suggests that large amounts of strongly adsorbed surface water are not required for the production of HONO, thus making it unlikely that the hydrolysis mechanism of NO₂ into HONO and HNO₃ in a surface liquid layer was occurring. The formation of HONO under dry conditions has been observed by many other groups.[23,33−35,37,38,42,46,47,50]

Longfellow at al. observed that when D₂O was passed over deactivated methane soot and subsequently exposed to NO₂,

Interaction of NO$_2$ with Hydrocarbon Soot

J. Phys. Chem. A, Vol. 111, No. 28, 2007 **6269**

DONO was generated.[24] The same experiment was performed with H$_2$O^{18} and only HONO and not HO^{18}NO was formed, indicating that the oxygen in water is not involved in the reaction.[24] The formation of DONO from the addition of D$_2$O does not unequivocally prove that water is directly involved in the reaction as pointed out by Lelievre et al., who observed an isotopic exchange reaction on kerosene soot by which D$_2$O was consumed on the surface to form HOD.[46] The exchange reaction could occur between D$_2$O and H$_2$O on the soot surface or with hydrogen-containing functional groups on the surface.[46] The deuterated functional groups, such as COD or COOD, could in turn be the source of DONO if they are involved in the reaction with NO$_2$ or if the HONO formed undergoes H−D exchange with these functional groups on the surface or with surface-bound D$_2$O.

Uptake Coefficient. Initial NO$_2$ uptake coefficients, γ_0, were calculated from eq 6, where the wall-loss rate constant is normalized to the SSA to geometric surface area ratio for the particular soot film:

$$\gamma_0 = \frac{2rk_w}{\omega}\left[\frac{A_{SSA}}{A_{geo}}\right]^{-1} \tag{6}$$

In eq 6, r is the radius of the Pyrex tube, k_w is the wall-loss rate constant, ω is the mean molecular speed of NO$_2$, A_{SSA} is the SSA of the sample, and A_{geo} is the geometric surface area of the sample. k_w is obtained from eq 7[63]

$$\frac{1}{k_{obs}} = \frac{1}{k_d} + \frac{1}{k_w} \tag{7}$$

where k_{obs} is the observed first-order rate coefficient for NO$_2$ loss and is given by eq 8

$$k_{obs} = \frac{d \ln S_{NO_2}}{dt} \tag{8}$$

where S_{NO_2} is the mass spectrometer signal for NO$_2$ and t is the time. k_d is the diffusion rate constant for NO$_2$ in helium and is given in eq 9

$$k_d = \frac{3.66}{r^2}\left[\frac{P_{He}}{D_{P,He}}\right]^{-1} \tag{9}$$

where P_{He} is the pressure of helium in the flow tube and $D_{P,He}$ is the gas diffusion coefficient for NO$_2$ in helium, which is 393 Torr cm^2 s^{-1}.[64]

Note that because soot is a porous solid, there is the possibility that not all of the soot mass is available for reaction. In that sense the BET-corrected uptake coefficients that we report are lower limits to the true uptake coefficient. That being said, we have chosen not to correct our initial uptake coefficients for pore diffusion,[65] in view of the structural complexity of soot, including lack of information on the porosity of our samples and soot's fractal nature.

The initial uptake coefficients for all three soot substrates were found to be $(3.9 \pm 1.9) \times 10^{-5}$. Table 4 summarizes literature values for the initial uptake coefficients for NO$_2$ on various BC substrates. The uptake coefficients range from 0.1 to 10^{-8}. Many of the earlier reported uptake coefficients were large, between 0.01 and 0.1, and were referenced to the geometric surface area of the sample. However, it is now known that this can lead to an overestimate of the uptake coefficient because the geometric surface area can be >3 orders of magnitude smaller than the SSA. In Table 4 we have normalized

the initial uptake coefficients referenced to the geometric surface area to the specific surface area, using the specific surface area of the soot substrate when it was available in the literature.

By so doing, the majority of the uptake coefficients are now in the 10^{-5} range. Ammann, Pöschl, and Rudich have developed an expression for the reactive uptake coefficient of gas-phase species due to surface reaction which demonstrates that the measured uptake coefficient will decrease with increasing gas-phase concentration of the reactants.[66] In the case of Kleffmann et al.[41] and Prezler-Prince et al.[42] the uptake experiments were conducted with very high NO$_2$ partial pressures, in the parts per million range, which will likely quickly saturate the soot samples and deactivate them, leading to the lower observed values for the uptake coefficients.

Heterogeneous Processing of the Surface. It is well-known that atmospheric aging processes will occur after soot is emitted to the atmosphere. The purpose of this section is to simulate some aspects of atmospheric oxidative aging by measuring the NO$_2$ uptake before and after ozonation of the soot. Several benzene soot samples were exposed to ozone at concentrations ranging from 3.9×10^{-3} to 8.6×10^{-5} Torr day^{-1} at room temperature. The specific surface areas of the benzene films were not directly measured but were estimated from the mass to SSA relationship that was determined to be 15 ± 1 m^2 g^{-1}. The uptake of NO$_2$ was first measured on half of the film, the entire film was then exposed to ozone, and finally the NO$_2$ uptake was measured on the other half of the film. Control experiments performed on films without processing showed that uptake coefficients and uptakes were reproducible to the $\pm 23\%$ level from half of the same film to the other. As shown in Table 5, the NO$_2$ uptake coefficient were reduced by $47 \pm 15\%$ after exposure to ozone, and Table 3 shows that the HONO yield remains the same after ozonation. The uptake coefficient after ozonation did not vary systematically with the ozone dose used in the experiment, which ranged by a factor of 40, when the 23% $1 - \sigma$ standard deviation is considered. The fact that the uptake does not fall to zero with high ozone exposures suggests that some sites that are reactive to NO$_2$ are not reactive to ozone. Similar deactivation of the surface with ozone exposure has been observed by Ammann et al.,[22] Kalberer et al.,[43] and Lelievre et al.[46] Also of relevance to atmospheric aging, Kleffmann et al. have shown that when commercial carbon samples are coated with $\sim 10^{14}$ molecules cm^{-2} of H$_2$SO$_4$, the HONO yields decrease to nearly zero and the yields of NO increase.[41] The decrease in the HONO yield could be due to its decomposition in the H$_2$SO$_4$ layer because partitioning of HONO to the carbon samples was observed to increase on H$_2$SO$_4$-coated carbon. Both the ozone exposure and the sulfate coating experiments show that atmospheric aging of the soot aerosols will have a significant impact on soot's ability to form HONO. The HONO generation capacities and the uptake coefficients reported both in this work and in the literature serve as upper limits to the behavior that will prevail in the atmosphere, being most representative of freshly emitted soot.

X-ray Photoelectron Spectroscopy Surface Analysis. To better define the overall mechanism for the reaction and to better evaluate the degree to which surface modification occurs, fresh hexane, decane, and benzene soot films were analyzed by XPS, along with benzene soot films following exposure to O$_3$ and NO$_2$. The analysis provided the surface elemental composition before and after exposure to NO$_2$ and O$_3$. Three sets of nitration experiments were conducted on benzene soot with a helium carrier gas: two with moderate NO$_2$ concentrations of 1.08×10^{-4} Torr for 28 min and 1.04×10^{-4} Torr for 19 min and one

TABLE 4: Summary of the Literature Data for the Initial Uptake Coefficient of NO_2 on Soot[a]

reference	substrate	P_{NO_2} (Torr)	γ_0	surface area	γ_{SSA} (corrected)
Tabor et al.[37]	Degussa FW2	10^{-3}	$(4.8 \pm 0.6) \times 10^{-2}$	geometric	$(1-4) \times 10^{-6}$
Tabor et al.[38]	Degussa FW2 FS 101 Printex 60	$(0.078-7.8) \times 10^{-3}$	$(6.4 \pm 2.0) \times 10^{-2}$	geometric	$(0.3-3.0) \times 10^{-6}$ $(0.1-1.2) \times 10^{-5}$ $(0.7-7.0) \times 10^{-5}$
Kalberer et al.[39]	graphite spark generator FW2 aerosol	6.2×10^{-7}	$(0.3-4.0) \times 10^{-4}$ $(2.4 \pm 1.4) \times 10^{-4}$	equivalent mobility diameter	
Rogaski et al.[40]	Degussa FW2	$(0.5-10) \times 10^{-3}$	0.11 ± 0.04	geometric	
Ammann et al.[22]	graphite spark generator	9.3×10^{-6}	1.1×10^{-2} 3.4×10^{-4} (exposed)	equivalent mobility diameter	
Gerecke et al.[23]	ethylene acetylene toluene	$2.3 \times 10^{-6} - 4.3 \times 10^{-4}$	$0.12-0.03$	geometric	
Longfellow et al.[24]	methane (295 K) methane (262 K) kerosene (295 K) kerosene (262 K) propane (262 K) hexane (262 K)	$(0.62-6.2) \times 10^{-5}$	$(2-4) \times 10^{-4}$ (exposed) 1.2×10^{-3} (fresh) $(2.4 \pm 1.5) \times 10^{-4}$ (fresh) $(5 \pm 1) \times 10^{-5}$ (exposed) $(2-4) \times 10^{-5}$ (exposed) $(1-1) \times 10^{-5}$ (exposed)	geometric	1.3×10^{-4} $(0.5-3.7) \times 10^{-5}$
Kleffmann et al.[41]	carbon black	$7.5 \times 10^{-4} - 2.9 \times 10^{-2}$	10^{-6}	BET	
Kirchner et al.[44]	spark discharge aerosol	$5 \times 10^{-5} - 7.8 \times 10^{-3}$	$10^{-3} - 10^{-6}$	BET	
Stadler et al.[34]	decane (oxidant rich) decane (fuel rich)	$2 \times 10^{-6} - 2.6 \times 10^{-4}$	0.1	geometric	5.5×10^{-5} 1.7×10^{-4}
Al-Abladeh and Grassian[50]	hexane	7.6×10^{-6}	5×10^{-5}	BET	
Prezler Prince et al.[42]	hexane Degussa FW2	$5-25 \times 10^{-3}$	$(2.4 \pm 0.6) \times 10^{-8}$ $(1.5 \pm 0.5) \times 10^{-8}$	BET	
Saathoff et al.[45]	graphite spark generator	7.8×10^{-5}	$\leq 4 \times 10^{-8}$	BET	
Salgado and Rossi[35]	hexane	$(0.62-3.4) \times 10^{-5}$	$(0.2-2.8) \times 10^{-3}$	geometric	$(2-3) \times 10^{-5}$
Lelievre et al.[46]	toluene kerosene hexane	$2.7 \times 10^{-5} - 3.4 \times 10^{-4}$	$(4.0 \pm 1.6) \times 10^{-5}$ $(5.0 \pm 2.0) \times 10^{-5}$ $(2.9 \pm 1.2) \times 10^{-5}$	BET	
Karagulian and Rossi[47]	decane (fuel-rich flame)	7×10^{-5}	$(3.0 \pm 0.6) \times 10^{-2}$	geometric	$(8.5 \pm 1.7) \times 10^{-5}$
this study	hexane decane benzene	$8 \times 10^{-6} - 1.4 \times 10^{-4}$	$(3.9 \pm 1.9) \times 10^{-5}$	BET	

[a] Values for γ_{SSA} (corrected) were obtained by dividing the γ_0 by the ratio of the geometric area of the sample and specific surface area of the sample. Values for the specific surface area of the substrates were taken from the publication when available or from the literature. Fresh samples refer to a substrate that has not been previously exposed to NO_2, whereas exposed samples have been previously exposed to NO_2.

TABLE 5: Calculated Uptake Coefficients on Benzene Soot before and after Ozonation[a]

sample mass (g)	γ_{SSA} (before ozonation)	ozone dose (Torr h^{-1})	γ_{SSA} (after ozonation)	decrease in γ_{SSA} after ozonation (%)
0.206	7.0×10^{-5}	7.6×10^{-3}	3.5×10^{-5}	50
0.348	4.1×10^{-4}	7.6×10^{-3}	3.1×10^{-5}	24
0.246	7.3×10^{-5}	2.3×10^{-3}	2.5×10^{-5}	66
0.410	4.4×10^{-5}	2.3×10^{-3}	1.7×10^{-5}	61
0.269	7.8×10^{-5}	3.4×10^{-2}	5.0×10^{-5}	35
0.342	6.0×10^{-5}	3.4×10^{-2}	3.2×10^{-5}	46
0.502	3.4×10^{-5}	3.4×10^{-2}	1.3×10^{-5}	60
0.292	4.5×10^{-5}	9.1×10^{-2}	2.7×10^{-5}	38
average				47 ± 15

[a] The specific surface area for the films was calculated from the mass to area relationship shown in Figure 3. Stated uncertainty is $1 - \sigma$ precision.

with a high NO_2 concentration of 2.2×10^{-2} Torr for 11 min. A fourth experiment used 1.6 Torr of O_2 in the carrier gas and a high NO_2 partial pressure of 1.4×10^{-2} Torr for 11.5 min. Two sets of ozonation experiments were conducted with 6.0×10^{-3} Torr of O_3 for 30 min and 1.6×10^{-2} Torr for 110 min.

The three soot substrates had similar surface elemental composition, which is consistent with their similar NO_2 uptake coefficients, SSAs, and HONO yields (Table 6). After ozonation, there was an increase in the amount of oxygen on the surface arising from the known ozonolysis mechanism.[2] After exposure to NO_2 at high concentrations, there was no statistical increase in the amount of nitrogen on the surface. This is consistent with the observed near unity yield of HONO production, which would not allow for any residual nitrogen to remain on the soot surface. The small increase of surface oxygen might reflect reactions that occur involving surface radical products subsequent to reaction 2. The simultaneous exposure of benzene soot to high concentrations of NO_2 and O_2, which did not lead to an additional increase in oxygen or nitrogen on the surface, was done to ensure that the presence of oxygen did not alter the reaction mechanism.

Reaction Mechanism. In this section we attempt to summarize our findings within the current understanding of the mechanism of this process. In particular, our results are all consistent with a mechanism by which the soot surface provides a H atom to NO_2 to form HONO.[23,24,34,35] In this manner, the overall oxidation state of the nitrogen atom decreases and the surface is oxidized to some degree. As mentioned in the Introduction we emphasized in this work a careful determination of the relative HONO to NO_2 sensitivities so that we could

Interaction of NO$_2$ with Hydrocarbon Soot

*J. Phys. Chem. A, Vol. 111, No. 28, 2007* **6271**

TABLE 6: Surface Elemental Ratios Obtained by X-ray Photoelectron Spectroscopy for Fresh Hexane, Decane, and Benzene Soot and for Benzene Soot Exposed to High and Low Concentrations[a] of NO$_2$ in a Helium Carrier Gas, to NO$_2$ in a Helium and O$_2$ Carrier Gas, and to O$_3$[b]

	surface elemental ratio (%)		
substrate	carbon	oxygen	nitrogen
decane	95.1 ± 0.5	4.6 ± 0.5	0.3 ± 0.1
hexane	93.0 ± 0.4	6.8 ± 0.5	0.2 ± 0.2
benzene	92.8 ± 0.5	6.9 ± 0.4	0.3 ± 0.1
benzene (low NO$_2$)	92.4 ± 0.5	7.2 ± 0.4	0.4 ± 0.2
benzene (high NO$_2$)	90.6 ± 0.6	8.6 ± 0.4	0.5 ± 0.3
benzene (high NO$_2$/O$_2$)	91.3 ± 0.6	8.1 ± 0.6	0.5 ± 0.1
benzene (O$_3$)	85.9 ± 0.6	13.4 ± 0.6	0.6 ± 0.3

[a] The experimental conditions were as follows: exposure to low concentrations of NO$_2$ consisted of 1.0×10^{-4} Torr of NO$_2$ for 19 min; exposure to high concentrations of NO$_2$ consisted of 2.2×10^{-2} Torr of NO$_2$ for 11 min; exposure to NO$_2$/O$_2$ mixture consisted of 1.4×10^{-2} Torr of NO$_2$ and 1.6 Torr of O$_2$ for 11.5 min; and exposure to O$_3$ consisted of 1.6×10^{-2} Torr of O$_3$ for 110 min. [b] The specific surface area for the films was calculated from the mass to area relationship shown in Figure 3. Stated uncertainty is $1 - \sigma$ precision.

accurately measure the HONO yield. The near unity yield that we observed lends strong support to the reaction proceeding through reaction 2 as opposed to the hydrolysis pathway of reaction 1. Although lower yields have been reported in the literature, it may be that these occur either when the NO$_2$ partial pressure is sufficiently high that self-reaction can occur, because the reaction was performed at lower temperatures, or when the reaction proceeds on soot surfaces that effectively lead to HONO reactive loss. In agreement with this mechanism are the findings that the reaction is noncatalytic or that the reactivity cannot be significantly regenerated after humidification of the soot sample or after the soot film has been allowed to rest for several days. Also, the XPS analysis indicates that nitrogen does not remain on the soot surface, which is consistent with the near unity yield of HONO.

Pryor and Lightsey have shown that NO$_2$ reacts with unsaturated hydrocarbons in the liquid phase with abstraction of the allylic hydrogen, leading to the direct formation of HONO:[67]

$$NO_2 + R-CH=CH-CH_2-R \rightarrow HONO +$$
$$R-CH=CH-\overset{\bullet}{C}H-R \quad (10)$$
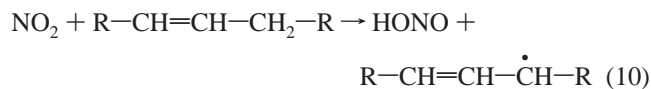
A mechanism based on eq 10 would also explain why soot produced from an oxidant-rich flame would have a lower HONO yield, because it would have a lower hydrogen content, relative to soot formed from a fuel-rich flame, as Stadler and Rossi have shown for decane soot.[34] If a similar mechanism occurs on soot, this would explain why ozonation, which involves the reaction of ozone with carbon−carbon double bonds, leads to a decrease in NO$_2$ uptake because loss of unsaturated C atoms will reduce the number of allylic H atoms and so reduce the ensuing stabilization of the radical formed in reaction 10. However, NO$_2$ and O$_3$ clearly do not react at entirely the same surface sites because we find that the deactivation of the soot surfaces with respect to NO$_2$ reaction via ozone exposure saturates (see Table 5); that is, with more ozone exposure, the degree of deactivation does not increase, indicative of loss of all the surface sites able to react with ozone.

We found that the soot surfaces can produce $(8.2 \pm 1.1) \times 10^{13}$ HONO molecules cm^{-2}, which is roughly a third of the total number of surface sites that might be present on a soot

surface. Ammann et al.,[22] Kirchner et al.,[44] and Kleffmann et al.[36] have found that nearly all adsorptive sites are reactive. Clearly not all of these sites are allylic moieties. On the other hand, a large fraction of aromaticity is expected to be present. Overall, we can say that a general reaction mechanism has the form given in reaction 2. This redox mechanism is consistent with the studies mentioned earlier,[23,24,34,35] such as those of Rossi and co-workers, which show that a more oxidized soot substrate produces less HONO than a surface formed from a fuel-rich flame.[34,35]

Atmospheric Implications. The formation of HONO from soot is potentially relevant for urban environments with high NO$_2$ concentrations, where HONO can build up overnight and then rapidly photolyze in the early morning to form HO$_x$. This rapid injection of OH can initiate other photochemical processes that are not yet working efficiently. The overall contribution of HONO photolysis to HO$_x$ formation can compete with O$_3$ and HCHO photolysis.[26] Other processes, including photoassisted surface chemistry involving NO$_2$, will likely dominate during the daytime.[68,69]

As a first cut, the amount of HONO that can potentially be formed from soot can be estimated from the amount of HONO formed per unit surface area measured in this study, that is, $(8.2 \pm 1.1) \times 10^{13}$ molecules cm^{-2}. This value is similar to that determined by others.[22,36,44] We prefer using this approach, which gives an absolute upper limit to HONO production, rather than a calculation based on our measured initial uptake coefficient, because the decrease in its value after exposure to NO$_2$ and soot aging must be accounted for. For soot particles in the atmosphere, which exist as agglomerates of much smaller primary particles, the specific surface area can be high but is not well-known. Assuming the density of these primary particles to be 2 g cm^{-3} and that their characteristic diameter is 30 nm,[70] the specific surface area is calculated to be 10^6 cm^2 g^{-1}. Thus, for a large soot loading of 20 μg m^{-3}, one can estimate that up to 1.6×10^9 molecules cm^{-3}, or just <0.1 ppbv, of HONO can be formed. Given that this does not take into consideration kinetic issues that might slow the release of HONO over multiple days, this estimate is an upper limit to the amount of HONO that can be formed. We conclude that the nighttime buildup of HONO cannot be attributed to the uptake of NO$_2$ on soot. Only if our estimate of the specific surface area of soot present in an urban environment is a gross underestimate, for example, if there is considerable surface roughness on the primary particles, would HONO production from soot be potentially important.

From a kinetic perspective, an early assessment by Ammann et al.[22] of HONO production rates was made using eq 11

$$\frac{d[HONO]}{dt} = \frac{\gamma \sigma \omega [NO_2]}{4} \quad (11)$$

with typical NO$_2$ concentrations, available soot surface area (σ), the mean molecular speed of NO$_2$ (ω), and length for nighttime (dt). Using their experimental kinetics values, Ammann et al. estimated that up to 10 ppbv of HONO in the boundary layer could be achieved over a nighttime.[22] Aumont et al. took the kinetics analysis further by considering both depositional losses of HONO and also deactivation of the soot as a result of NO$_2$ processing, as observed both in this study and in most others.[46,71] The modeling result is that the overall rate of HONO production is likely to be important to HO$_x$/ozone levels only if deactivation of the soot with NO$_2$ uptake does not occur. However, from both this work and earlier studies, it is now apparent that this

is a noncatalytic reaction that is controlled primarily by the number of reactive sites on the surface.

Finally, we have shown, along with others,[22,43,46] that oxidation of the soot film with ozone will decrease the reactivity of the soot film. Lelievre et al.[46] have shown the same with exposure to ambient air, and Kleffmann et al. have demonstrated that a rough monolayer (10^{14} molecules cm^{-2}) coverage of H$_2$SO$_4$, which one would expect after atmospheric aging, reduces the amount of HONO produced.[41]

A comparison of the direct HONO emission from vehicles and the amount of HONO that could be produced from the black carbon emitted from vehicles shows that direct emissions could be more important as HONO sources. For example, the black carbon emission index of 1140 ± 160 mg of black carbon kg^{-1} of fuel for heavy-duty diesel trucks calculated by Miguel et al.[72] equates to 7 mg of HONO kg^{-1} of fuel, if we assume a specific surface area of 10^6 cm^2 g^{-1} and that 8.2×10^{13} molecules of HONO are generated per cm^{-2}. This is significantly smaller than the HONO emission index of 115 ± 10 mg of HONO kg^{-1} of fuel for a diesel truck engine calculated by Kurtenbach et al.[31]

All of this suggests that only under certain specific conditions of high NO$_2$ concentrations and high and fresh soot loadings with large surface areas will the uptake of NO$_2$ on soot contribute significantly to the production and buildup of nighttime HONO. Such environments include street canyons or tunnel environments. Other HONO production mechanisms, such as the hydrolysis of NO$_2$ in surface adsorbed water on ground surfaces, may also contribute to the observed nighttime buildup of HONO. This is plausible because the maximum surface area to volume ratio that can be attributed to ground surfaces in the boundary layer, with a minimum 100 m mixing height, is 10^{-2} cm^{-1}, considerably more than that due to aerosols.[22]

References and Notes

(1) Lary, D. J.; Lee, A. M.; Toumi, R.; Newchurch, M. J.; Pirre, M.; Renard, J. B. *J. Geophys. Res.* **1997**, *102*, 3671.

(2) Finlayson-Pitts, B. J.; Pitts, J. N. J. *Chemistry of the Upper and Lower Atmosphere: Theory, Experiments and Applications*; Academic Press: San Diego, CA, 2000.

(3) *Climate Change 2001: The Scientific Basis: Contribution of Working Group I to the Third Assessment Report of the Intergovernmental Panel on Climate Change*; Houghton, J. T., Ed.; Cambridge University Press: Cambridge, U.K., 2001.

(4) Clarke, A. D.; Weiss, R. E.; Charlson, R. J. *Sci. Total Environ.* **1984**, *36*, 97.

(5) Andreae, M. O.; Andreae, T. W.; Ferek, R. J.; Raemdonck, H. *Sci. Total Environ.* **1984**, *36*, 73.

(6) Cadle, S. H.; Dash, J. M. *Atmos. Environ.* **1988**, *22*, 1373.

(7) Clarke, A. D. *Aerosol Sci. Technol.* **1989**, *10*, 161.

(8) Hansen, A. D. A.; Bodhaine, B. A.; Dutton, E. G.; Schnell, R. C. *Geophys. Res. Lett.* **1988**, *15*, 1193.

(9) *Particulate Carbon, Atmospheric Life Cycle*; Wolf, G. T., Klimisch, R. L., Eds.; Plenum Press: New York, 1982.

(10) Gray, H. A.; Cass, G. R.; Huntzicker, J. J.; Heyerdahl, E. K.; Rau, J. A. *Sci. Total Environ.* **1984**, *36*, 17.

(11) Grosjean, D. *Sci. Total Environ.* **1984**, *32*, 133.

(12) Akhter, M. S.; Chughtai, A. R.; Smith, D. M. *Appl. Spectrosc.* **1985**, *39*, 154.

(13) Akhter, M. S.; Chughtai, A. R.; Smith, D. M. *Appl. Spectrosc.* **1985**, *39*, 143.

(14) Akhter, M. S.; Chughtai, A. R.; Smith, D. M. *Appl. Spectrosc.* **1991**, *45*, 653.

(15) Chughtai, A. R.; Brooks, M. E.; Smith, D. M. *J. Geophys. Res.* **1996**, *101*, 19505.

(16) Chughtai, A. R.; Williams, G. R.; Atteya, M. M. O.; Miller, N. J.; Smith, D. M. *Atmos. Environ.* **1999**, *33*, 2679.

(17) Chughtai, A. R.; Smith, D. M.; Miller, N. J.; Pitts, J. R. *J. Atmos. Chem.* **1999**, *34*, 259.

(18) Strom, J.; Ohlsson, S. J. *Soot Formation in Combustion: Mechanism and Models*; Springer: Berlin, Germany, 1994.

(19) Hauglustaine, D. A.; Ridley, B. A.; Solomon, S.; Hess, P. G.; Madronich, S. *Geophys. Res. Lett.* **1996**, *23*, 2609.

(20) Lary, D. J.; Shallcross, D. E.; Toumi, R. *J. Geophy. Res.* **1999**, *104*, 15929.

(21) Nienow, A. M.; Roberts, J. T. *Annu. Rev. Phys. Chem.* **2006**, *57*, 105.

(22) Ammann, M.; Kalberer, M.; Jost, D. T.; Tobler, L.; Rossler, E.; Piguet, D.; Gäggeler, H. W.; Baltensperger, U. *Nature* **1998**, *395*, 157.

(23) Gerecke, A.; Thielmann, A.; Gutzwiller, L.; Rossi, M. J. *Geophys. Res. Lett.* **1998**, *25*, 2453.

(24) Longfellow, C. A.; Ravishankara, A. R.; Hanson, D. R. *J. Geophy. Res.* **1999**, *104*, 13833.

(25) Lammel, G.; Cape, J. N. *Chem. Soc. Rev.* **1996**, *25*, 361.

(26) Alicke, B.; Platt, U.; Stutz, J. *J. Geophy. Res.* **2002**, *107*, 8196.

(27) Ren, X. R.; Harder, H.; Martinez, M.; Lesher, R. L.; Oliger, A.; Shirley, T.; Adams, J.; Simpas, J. B.; Brune, W. H. *Atmos. Environ.* **2003**, *37*, 3627.

(28) Acker, K.; Moller, D.; Wieprecht, W.; Meixner, F. X.; Bohn, B.; Gilge, S.; Plass-Dulmer, C.; Berresheim, H. *Geophys. Res. Lett.* **2006**, *33*, L02809.

(29) Kleffmann, J.; Gavriloaiei, T.; Hofzumahaus, A.; Holland, F.; Koppmann, R.; Rupp, L.; Schlosser, E.; Siesse, M.; Wahner, A. *Geophys. Res. Lett.* **2005**, *32*, L05818.

(30) Kirchstetter, T. W.; Harley, R. A.; Littlejohn, D. *Environ. Sci. Technol.* **1996**, *30*, 2843.

(31) Kurtenbach, R.; Becker, K. H.; Gomes, J. A. G.; Kleffmann, J.; Lörzer, J. C.; Spittler, M.; Wiesen, P.; Ackermann, R.; Geyer, A.; Platt, U. *Atmos. Environ.* **2001**, *35*, 3385.

(32) Finlayson-Pitts, B. J.; Wingen, L. M.; Sumner, A. L.; Syomin, D.; Ramazan, K. A. *Phys. Chem. Chem. Phys.* **2003**, *5*, 223.

(33) Alcala-Jornod, C.; van den Bergh, H.; Rossi, M. *Phys. Chem. Chem. Phys.* **2000**, *2*, 5584.

(34) Stadler, D.; Rossi, M. J. *Phys. Chem. Chem. Phys.* **2000**, *2*, 5420.

(35) Salgado, M. S.; Rossi, M. J. *Int. J. Chem. Kinet.* **2002**, *34*, 620.

(36) Kleffmann, J.; Wiesen, P. *Atmos. Chem. Phys.* **2005**, *5*, 77.

(37) Tabor, K.; Gutzwiller, L.; Rossi, M. J. *Geophys. Res. Lett.* **1993**, *20*, 1431.

(38) Tabor, K.; Gutzwiller, L.; Rossi, M. J. *J. Phys. Chem.* **1994**, *98*, 6172.

(39) Kalberer, M.; Tabor, K.; Ammann, M.; Weingartner, E.; Piguet, D.; Rossler, E.; Jost, D.; Turler, A.; Gäggeler, H.; Baltensperger, U. *J. Phys. Chem.* **1996**, *100*, 15487.

(40) Rogaski, C. A.; Golden, D. M.; Williams, L. R. *Geophys. Res. Lett.* **1997**, *24*, 381.

(41) Kleffmann, J.; Becker, K. H.; Lackhoff, M.; Wiesen, P. *Phys. Chem. Chem. Phys.* **1999**, *1*, 5443.

(42) Prezler-Prince, A.; Wade, J. L.; Grassian, V. H.; Kleiber, P. D.; Young, M. A. *Atmos. Environ.* **2002**, *36*, 5729.

(43) Kalberer, M.; Ammann, M.; Arens, F.; Gäggeler, H. W.; Baltensperger, U. *J. Geophy. Res.* **1999**, *104*, 13825.

(44) Kirchner, U.; Scheer, V.; Vogt, R. *J. Phys. Chem. A* **2000**, *104*, 8908.

(45) Saathoff, H.; Naumann, K. H.; Riemer, N.; Kamm, S.; Mohler, O.; Schurath, U.; Vogel, H.; Vogel, B. *Geophys. Res. Lett.* **2001**, *28*, 1957.

(46) Lelievre, S.; Bedjanian, Y.; Laverdet, G.; Le, Bras, G. *J. Phys. Chem. A* **2004**, *108*, 10807.

(47) Karagulian, F.; Rossi, M. J. *J. Phys. Chem. A* **2007**, *111*, 1914.

(48) De Santis, F.; Allegrini, I. *Atmos. Environ.* **1992**, *26A*, 3061.

(49) Arens, F.; Gutzwiller, L.; Gaeggeler, H. W.; Ammann, M. *Phys. Chem. Chem. Phys.* **2002**, *4*, 3684.

(50) Al-Abadleh, H. A.; Grassian, V. H. *J. Phys. Chem. A* **2000**, *104*, 11926.

(51) Brunauer, S.; Emmett, P. H.; Teller, E. *J. Am. Chem. Soc.* **1938**, *60*, 309.

(52) Sing, K. S. W.; Everett, D. H.; Haul, R. A. W.; Moscou, L.; Pierotti, R. A.; Rouquerol, J.; Siemieniewska, T. *Pure Appl. Chem.* **1985**, *57*, 603.

(53) Aubin, D. G.; Abbatt, J. P. *J. Phys. Chem. A* **2003**, *107*, 11030.

(54) Aubin, D. G.; Abbatt, J. P. *Environ. Sci. Technol.* **2006**, *40*, 179.

(55) Sharkey, A. G.; Shultz, J. L. J.; Friedel, R. A. *Analytical Methods in Mass Spectrometry*; Bulletin 634; U.S. Bureau of Mines: Washington, DC, 1967.

Interaction of NO$_2$ with Hydrocarbon Soot

J. Phys. Chem. A, Vol. 111, No. 28, 2007 **6273**

(56) Abbatt, J. P. *Geophys. Res. Lett.* **1997**, *24*, 1479.

(57) Febo, A.; Perrino, C.; Gherardi, M.; Sparapani, R. *Environ. Sci. Technol.* **1995**, *29*, 2390.

(58) Wingen, L. M.; Barney, W. S.; Lakin, M. J.; Brauers, T.; Finlayson-Pitts, B. J. *J. Phys. Chem. A* **2000**, *104*, 329.

(59) IUPAC Subcommittee for Gas Kinetic Data Evaluation, available at http://www.iupac-kinetic.ch.cam.ac.uk/.

(60) Fan, X. H.; Brook, J. R.; Mabury, S. A. *Environ. Sci. Technol.* **2003**, *37*, 3145.

(61) Schiff, H. I.; Mackay, G. I.; Castledine, C.; Harris, G. W.; Tran, Q. *Water, Air Soil Pollut.* **1986**, *30*, 105.

(62) Choi, W.; Leu, M.-T. *J. Phys. Chem. A* **1998**, *102*, 7618.

(63) Pöschl, U.; Canagaratna, M.; Jayne, J. T.; Molina, L. T.; Worsnop, D. R.; Kolb, C. E.; Molina, M. J. *J. Phys. Chem. A* **1998**, *102*, 10082.

(64) Thornberry, T.; Abbatt, J. P. D. *Phys. Chem. Chem. Phys.* **2004**, *6*, 84.

(65) Keyser, L. F.; Moore, S. B.; Leu, M.-T. *J. Phys. Chem.* **1991**, *95*, 5496.

(66) Ammann, M.; Pöschl, U.; Rudich, Y. *J. Phys. Chem. A* **2003**, *107*, 351.

(67) Pryor, W. A.; Lightsey, J. W. *Science* **1981**, *214*, 435.

(68) George, C.; Strekowski, R. S.; Kleffmann, J.; Stemmler, K.; Ammann, M. *Faraday Discuss.* **2005**, *130*, 195.

(69) Stemmler, K.; Ammann, M.; Donders, C.; Kleffmann, J.; George, C. *Nature* **2006**, *440*, 195.

(70) Seinfeld, J. H.; Pandis, S. N. *Atmospheric Chemistry and Physics: from Air Pollution to Climate Change*; Wiley-Interscience: New York, 1998.

(71) Aumont, B.; Madronich, S.; Ammann, M.; Kalberer, M.; Baltensperger, U.; Hauglustaine, D.; Brocheton, F. *J. Geophy. Res.* **1999**, *104*, 1729.

(72) Miguel, A. H.; Kirchstetter, T. W.; Harley, R. A.; Hering, S. V. *Environ. Sci. Technol.* **1999**, *32*, 450.